Research Article Vol. 34, No. 9 / September 2017 / Journal of the Optical Society of America B 1855

Journal of the Optical Society of America B

OPTICAL PHYSICS

Thermal tuning of spectral emission from optically trapped liquid-crystal droplet resonators

Alexandr Jonáš,[1,2,*] Zdeněk Pilát,[2] Jan Ježek,[2] Silvie Bernatová,[2] Tomáš Fořt,[2] Pavel Zemánek,[2] Mehdi Aas,[3] and Alper Kiraz[4,5]

[1]Department of Physics, Istanbul Technical University, Maslak, 34469 Istanbul, Turkey
[2]Institute of Scientific Instruments of the CAS, v.v.i., Královopolská 147, 61264 Brno, Czech Republic
[3]Complex Photonic Systems, MESA+ Institute for Nanotechnology, University of Twente, Enschede 7500 AE, The Netherlands
[4]Department of Physics, Koç University, Rumelifeneri Yolu, Sariyer, 34450 Istanbul, Turkey
[5]Department of Electrical and Electronics Engineering, Koç University, Rumelifeneri Yolu, Sariyer, 34450 Istanbul, Turkey
*Corresponding author: ajonas@itu.edu.tr

Received 11 May 2017; revised 13 July 2017; accepted 14 July 2017; posted 17 July 2017 (Doc. ID 295240); published 9 August 2017

Surfactant-stabilized emulsion droplets of liquid crystals (LCs) suspended in water and labeled with a fluorescent dye form active, anisotropic optofluidic microresonators. These microresonators can host whispering gallery modes (WGMs), high-quality morphology-dependent optical resonances that are supported due to the contrast of refractive index between the LC droplets and the surrounding aqueous medium. In addition, owing to the refractive index contrast, such LC emulsion droplets can be stably trapped in three dimensions using optical tweezers, enabling long-term investigation of their spectral characteristics. We explore various combinations of fluorescently dyed LC droplets and host liquid-surfactant systems and show that the WGM emission spectra of optical resonators based on optically trapped LC emulsion droplets can be largely and (almost) reversibly tuned by controlled changes of the ambient temperature. Depending on the actual range of temperature modulation and LC phase of the studied droplet, thermally induced effects can either lead to phase transitions in the LC droplets or cause modifications of their refractive index profile without changing their LC phase. Our results indicate feasibility of this approach for creating miniature thermally tunable sources of coherent light that can be manipulated and stabilized by optical forces.

OCIS codes: (140.3945) Microcavities; (160.3710) Liquid crystals; (350.4855) Optical tweezers or optical manipulation; (130.6010) Sensors; (130.3120) Integrated optics devices.

https://doi.org/10.1364/JOSAB.34.001855

1. INTRODUCTION

Optofluidics—a rapidly developing scientific discipline based on the theoretical foundations and experimental techniques of physics of fluids, chemistry, and optics—utilizes optical and mechanical properties of fluids for creating unique reconfigurable optical systems inconceivable with conventional solid-state materials [1,2]. Optical resonators (cavities) with precisely defined spectral characteristics are among the most critical components of integrated optofluidic systems, as they are indispensable for implementing wavelength-selective optical devices, such as add-drop filters, attenuators, or photonic circuit switches [3]. Active fluid-based optical resonators containing a suitable gain medium then serve as the starting point for developing integrated optofluidic sources of laser light [4–8]. Liquid microdroplets with nearly perfectly spherical geometry and atomically smooth surfaces, surrounded by a medium with a low refractive index, are capable of hosting high-quality morphology-dependent optical resonances—whispering gallery modes (WGMs)—which arise due to total internal reflection of light from the inner surface of the droplet [9,10]. In a WGM circulating within the droplet, a major fraction of the light intensity is confined to the proximity of the droplet surface, which leads to high energy densities in this region [11,12]. Spectral positions of the cavity WGMs then depend sensitively on the shape and size of the droplet and on the refractive index of both the droplet liquid and the surrounding medium. Since all these parameters can be relatively easily controlled and adjusted, self-assembled optofluidic cavities represented by liquid droplets allow for straightforward tuning of their optical resonant spectra [13–18]. Furthermore, strong response of the droplet-based optofluidic cavities to environmental conditions has been recently employed for building novel types of chemical sensors [19,20].

Liquid crystals (LCs) are complex fluids with material characteristics combining long-range organization found in crystalline solids with liquid-like fluidity that opens up the possibility

of controlling the molecular orientation using moderate external perturbations. In general, organization of LC molecules in any given state of the bulk LC fluid is characterized by the orientation of the molecular director field, which depends strongly on the physicochemical nature of the LC molecules and confinement geometry of the LC fluid [21–23]. Dielectric anisotropy of individual LC molecules, in connection with their bulk and/or surface organization, then manifest themselves through optical birefringence of the LC fluid that can be adjusted by controlling orientation of LC molecules using external stimuli, such as electric field, mechanical stress, or temperature changes. Consequently, anisotropic optofluidic laser resonators formed by LC droplets offer additional paths for tuning the spectral profile of lasing emission [24–27]. Recently, emulsion droplets of nematic liquid crystals have been exploited as temperature sensors with the sensor readout signal represented by spectral shifting of the WGM positions resulting from the changes of the ambient temperature [28]. Moreover, the transitions from smectic-A to nematic phase induced in individual micrometer-sized LC droplets by sample heating have been monitored by recording the temperature-dependent spectral width of the droplet WGMs [29].

In addition, some LC phases possess chiral properties associated with the helical character of the long-range supramolecular organization that stems either from the inherent chirality of LC molecules or from the presence of a suitable chiral dopant in the LC fluid [30]. Helical organization of anisotropic LC molecules in the bulk fluid phase leads to periodic modulation of the refractive index, which is a prerequisite for the existence of photonic bandgap in the material [31]. Depending on the actual chiral LC phase and boundary conditions imposed on the liquid-crystalline material, this photonic bandgap can be one-dimensional to three-dimensional and—with a suitable pitch of the helical structure—it can lie in the visible part of the spectrum. Such chiral LC materials with photonic bandgap properties hold great promise for optofluidic applications as they enable development of largely tunable passive and active optical components and mirrorless lasers with low pump threshold, small cavity dimensions, and large output power [32]. Functional Bragg-type optical microcavities based on surface-supported emulsion microdroplets of chiral cholesteric LCs have been recently demonstrated by Humar and Musevic [33] and cholesteric LC droplets have been also used for selective chemical and biological sensing [34].

In this paper, we report on the development and characterization of tunable optofluidic resonators based on dye-doped emulsion droplets of nematic liquid crystals suspended in an immiscible aqueous host liquid with the refractive index smaller than the refractive index of the LC liquid, thus supporting WGM resonances. The contrast of refractive index necessary for supporting WGMs in the droplets also enables stable spatial confinement of the studied droplets in optical tweezers and full dynamic control over their position, which adds large flexibility to the spectroscopic experiments with individual droplets [35–37]. In addition, working with LC droplet cavities that are optically trapped within a liquid environment permits straightforward *in situ* adjustment of the chemical composition of the environment. We explore various combinations of fluorescently dyed LC droplets and host liquid-surfactant systems and show that WGM emission spectrum of an LC droplet-based resonator can be largely and (almost) reversibly tuned by controlled variations of the ambient temperature. We characterize the changes of WGM emission patterns of the droplets during large temperature modulation leading to phase transitions in the droplets and during small, localized temperature adjustments that are sufficient to modify the refractive index profile of the droplets without changing their LC phase.

2. EXPERIMENTAL SETUP

The experimental setup used for WGM spectroscopy of individual optically trapped emulsion droplets of LCs is shown in Fig. 1. During spectral acquisition, studied droplets were spatially confined using a single-beam optical trap (optical tweezers) generated by focusing a near-infrared cw laser beam (wavelength 1064 nm, typical trapping power less than 100 mW at the sample; YLR-10-LP-Y12, IPG Photonics) with a high numerical aperture oil-immersion microscope objective (magnification 100 ×, NA = 1.4; UplanSapo, Olympus). The trapping beam was expanded with a two-lens telescope to overfill the back aperture of the objective lens. In addition, transversal motion of the first lens of the telescope could be used for positioning of the optical trap in the field of view [38]. In order to excite fluorescence in the optically trapped LC droplets, the droplets were pumped by a pulsed green laser beam (wavelength 532 nm, pulse duration 9 ns; Minilite II, Continuum) focused near the droplet rim. A single pump pulse was sufficient to acquire an emission spectrum. The intensity of WGM emission from the droplets could be optimized by moving the optical trap with respect to the excitation beam focus. During the course of an experiment, we generally observed a gradual decrease of intensity of the recorded emission spectra due to photobleaching of the used fluorescent dye. The actual level of the light-induced dye bleaching depended on the used pump energy, the concentration

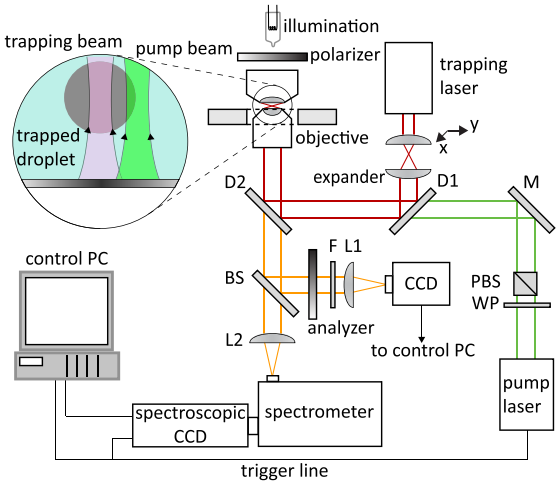

Fig. 1. Experimental setup for optical spectroscopy of emulsion droplets of LCs. The inset shows the detail of an optically trapped droplet with the pump laser beam positioned on the droplet rim. BS, beam splitter; D1, D2, dichroic mirrors; F, bandpass filter; L1, L2, lenses; M, mirror; PBS, polarizing beam splitter; and WP, half-wave plate.

of the dye in the droplets, the type of the used liquid crystal, and the type and concentration of the used surfactant. Typically, we were able to record thousands of droplet emission spectra from an individual optically trapped droplet before the signal-to-noise ratio of the acquired spectra became too low. Fluorescence light emitted from the excited droplets was collected using the same microscope objective that was used for focusing the trapping and pump beams and subsequently analyzed by an imaging spectrometer (focal length 300 mm; SpectraPro 2300i, Acton). Simultaneously with the spectral acquisition, studied LC droplets could be observed using an inverted optical microscope equipped with a polarizer and analyzer with adjustable rotation angle. This enabled implementation of polarization microscopy, which is especially well suited for examining the actual liquid-crystalline phase of the droplets during the experiment. Individual components of the setup were synchronized using a custom written LabView code.

Figure 2 shows the prototype of a polydimethylsiloxane (PDMS) microfluidic chip which allowed *in situ* control of temperature of the studied LC emulsion. To this end, the chip contained a resistive-wire coil (heating wire) embedded in the PDMS block forming the body of the chip. This resistive wire coil was connected to an external DC power supply and—by controlling the power supply voltage—the amount of heat generated in the wire could be adjusted. The actual temperature of the chip could be monitored by a platinum resistance probe PT100 inserted into a dedicated inlet in the chip. Studied LC emulsions were loaded into the working channel in the chip (width ~200 μm, height ~50 μm), which was formed between the PDMS block and a standard microscope coverslip. This coverslip, which was irreversibly bonded to the bottom surface of the PDMS block, enabled optical access to the channel using an inverted optical microscope configuration. In order to prevent distortions of the chip during heating which stem from different heat expansion coefficients of PDMS and glass coverslip, a thick glass plate was embedded in the PDMS block to increase its bending rigidity. During a typical heating experiment, the studied droplet was confined by optical tweezers inside the working channel, with the pump beam focus positioned at the droplet edge (see inset in Fig. 1). Occasional streaming of the host liquid in the channel could generate hydrodynamic forces that could eventually pull the droplet out of the trap, thus disturbing the experiment. To increase the stability of the trapped droplet, thin flexible tubing was connected to both the inlet and the outlet of the chip. By manipulating the free ends of both pieces of tubing, hydrostatic pressure difference across the channel could be kept close to zero, thus eliminating the bulk fluid flow.

As an alternative to heating the whole chip containing the studied LC emulsion, droplet temperature could also be

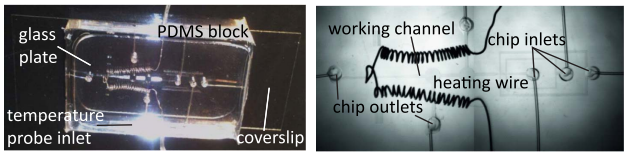

Fig. 2. Microfluidic chip used for controlled heating of liquid crystal emulsions during spectroscopic experiments.

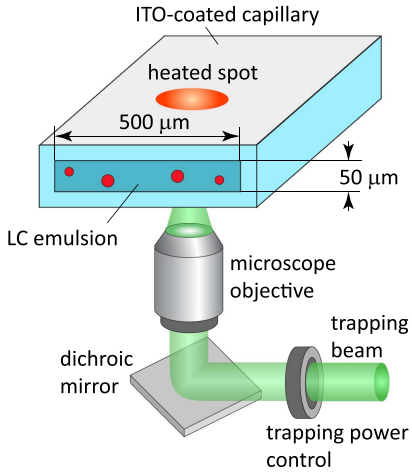

Fig. 3. Schematics of experimental configuration used for tuning of emission spectra of optically trapped isotropic LC emulsion droplets by changing the power of the trapping laser beam. Absorption of the trapping laser light creates heated spots at the top and bottom surfaces of an ITO-coated capillary which forms the sample chamber.

adjusted by gradual modification of the optical trapping power. This approach enabled a faster, more precise, and more localized control of temperature of the studied trapped droplet, without affecting significantly neighboring droplets flowing in the chip outside the region illuminated by the focused trapping beam. We tested two different approaches for heating the droplets by the absorption of the trapping laser light. For experiments carried out with LC droplets in the isotropic phase (see discussion of the various studied LC phases in Section 3), we used a sample chamber constructed from a glass capillary of rectangular cross section whose top and bottom surfaces were coated with transparent, partially absorptive indium-tin oxide (ITO) layers (see Fig. 3). Absorption of the trapping laser light in ITO layers then created heated spots at the top and bottom surfaces of the capillary, which caused localized heating of the LC emulsion. For experiments carried out with LC droplets in the radial phase, which are more sensitive to temperature changes, the droplets were placed in the standard chip shown in Fig. 2 with external heating turned off and the local temperature was controlled simply by varying the trapping laser power, without any additional absorbing elements present in the sample chamber.

3. EMULSION SYSTEMS OF LIQUID CRYSTALS USED IN WGM SPECTROSCOPIC EXPERIMENTS

Finding a suitable combination of liquid crystal, fluorescent dye, surfactant, and host liquid that allows generation of stable LC emulsion droplets in a well-defined liquid-crystalline phase is a necessary prerequisite for optical experiments involving the study of emission from LC droplet-based optofluidic microcavities. Constraints on the used materials are mainly

- immiscibility of the used LC with the host liquid, which determines the stability of the droplet size during the experiment;

• sufficient contrast of refractive indices of the LC (n_{LC}) and the host liquid (n_{host}) required to support resonant WGMs in the emulsion droplets ($n_{LC} > n_{host}$); and
• good solubility of the used dye in the LC and minimal influence of the dye on the LC molecular director field.

To address these issues, we have prepared and characterized the following emulsions of dye-doped LCs in an aqueous host liquid ($n_{host} = 1.33$):

(a) 5CB (4′-Pentyl-4-biphenylcarbonitrile) LC (refractive index in isotropic phase $n_{LC} = 1.58$ at 640 nm) +1%w/w Nile Red fluorescent dye +4 mM sodium dodecyl sulfate (SDS) ionic surfactant. At room temperature around ~23°C, this material combination produces LC emulsion droplets with **radial** orientation of the molecular director [see a typical droplet image in the inset of Fig. 4(a)].
(b) 5CB +1%w/w Nile Red +0.7 mM SDS. At room temperature around ~23°C, this material combination produces LC emulsion droplets with **bipolar** orientation of the molecular director [see a typical droplet image in the inset of Fig. 4(b)].
(c) 5CB +1%w/w Nile Red + > 1200 mg/L Triton X-100 nonionic surfactant. At room temperature above ~23°C, this material combination produces LC emulsion droplets in **isotropic** (melted) phase [see a typical droplet image in the inset of Fig. 4(c)]. The fact that the melting of 5CB droplets from nematic to isotropic phase in the presence of a high concentration of Triton X-100 in the host liquid occurs at a relatively low ambient temperature stems from the partial solubility of nonionic Triton X-100 in 5CB (the hydrophile–lipophile balance of Triton X-100 is 13.5 [39]). Consequently, the surfactant molecules can penetrate the droplets, acting as internal impurities, which disrupt the LC organization and depress the phase-transition temperature with respect to that of the pure LC fluid [40].
(d) 5CB +1%w/w Nile Red +300 mg/L Triton X-100. At room temperature around ~23°C, this material combination produces LC emulsion droplets with **bipolar** orientation of the molecular director [see a typical droplet image in the inset of Fig. 4(d)].
(e) PCBN (4-[*trans*-4-Pentylcyclohexyl]benzonitrile) LC (refractive index in isotropic phase $n_{LC} = 1.58$ at 640 nm) +1%w/w Nile Red +1200 mg/L Triton X-100. At room temperature around ~23°C, this material combination produces LC emulsion droplets with **bipolar** orientation of the molecular director [see a typical droplet image in the inset of Fig. 4(e)].
(f) 7CB (4′-Heptyl-4-biphenylcarbonitrile) LC (refractive index in isotropic phase $n_{LC} = 1.56$ at 640 nm) +1%w/w Nile Red +1200 mg/L Triton X-100. At room temperature around ~23°C, this material combination produces LC emulsion droplets with **bipolar** orientation of the molecular director [see a typical droplet image in the inset of Fig. 4(f)].

All LC samples and Nile Red fluorescent dye used in the experiments were supplied by Sigma-Aldrich and used as received. The emulsions were prepared by mixing fluorescently dyed LCs with surfactant/water solutions in 1∶100 volume ratio and gentle manual agitation of the mixture. Depending on the particular combination of LC and host liquid/surfactant and on the storage conditions, the emulsions were stable and usable for spectroscopic experiments on the time scale ranging from several days to several months.

Droplet emission spectra shown in Fig. 4 reflect significant differences in the internal long-range order of LC molecules within the droplets in individual studied cases. With the radial orientation of the LC molecular director [Fig. 4(a)], LC droplets display complete spherical symmetry. Thus, all WGMs with the same angular mode number l, which is approximately equal to the number of light wavelengths that fit into the

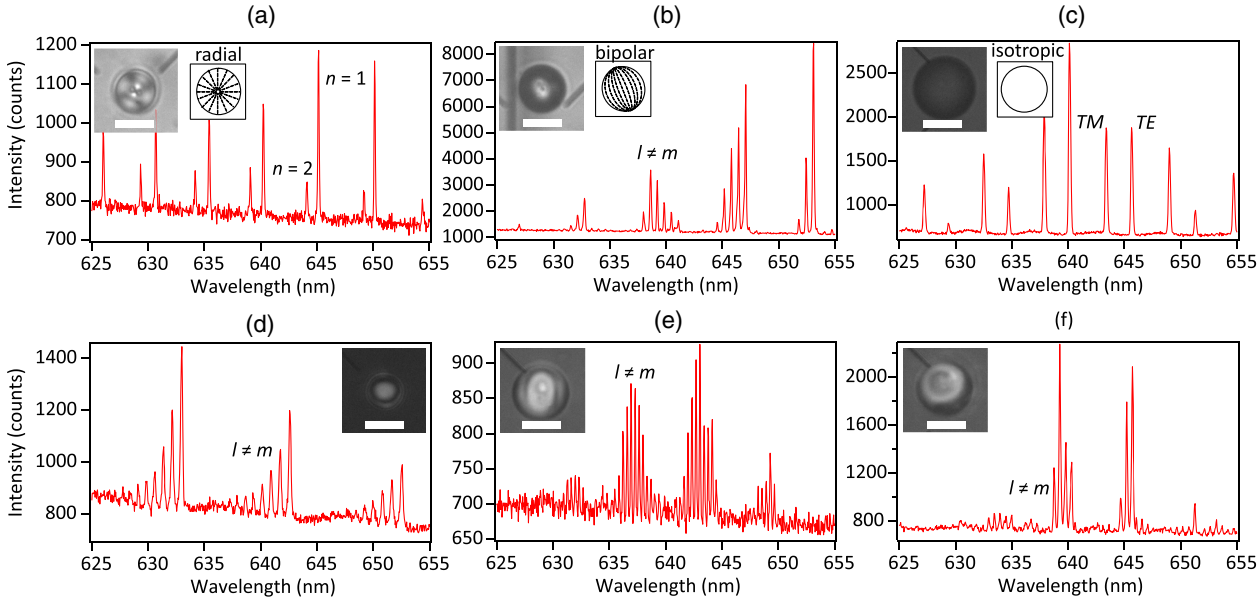

Fig. 4. WGM emission spectra recorded from various dye-doped emulsion droplets of liquid crystals pumped with a pulsed laser beam. (a) 5 CB + Nile Red + 4 mM SDS; (b) 5 CB + Nile Red + 0.7 mM SDS; (c) 5 CB + Nile Red+ > 1200 mg/L Triton X-100; (d) 5 CB + Nile Red + 300 mg/L Triton X-100; (e) PCBN + Nile Red + 1200 mg/L Triton X-100; (f) 7 CB + Nile Red + 1200 mg/L Triton X-100. Insets show typical droplet images acquired for the given emulsion system using polarization microscopy [parts (a)–(f)] and schematics of spatial distribution of the LC molecular director [parts (a)–(c)]. All scale bars: 10 μm.

resonant light path around the droplet circumference, are frequency-degenerate [11]. Radial orientation of the LC director is associated with strong birefringence, which causes a large difference in the ordinary refractive index n_o experienced by TE-polarized modes (electric field tangential to the droplet surface) and the extraordinary refractive index n_e experienced by TM-polarized modes (electric field normal to the droplet surface). Since $n_o < n_e$ due to the rod-like shape of all studied LC molecules [41], in small radial LC droplets with diameters ~10 μm, the contrast of the effective refractive indices between the droplet and the host liquid with the refractive index n_{host} is sufficient to support TM-polarized modes (relative refractive index n_e/n_{host}) but not TE-polarized modes (relative refractive index n_o/n_{host}), which, therefore, are virtually absent from the spectrum. As the droplet size grows, the quality factor (Q-factor) of the droplet WGM resonances, which is inversely proportional to the width $\Delta\lambda$ of the resonant peak, generally increases [11] and the TE-polarized modes are eventually expected to appear in the WGM spectrum. However, due to the low relative refractive index n_o/n_{host}, their amplitude and Q-factor are always smaller than the amplitude and Q-factor of the corresponding TM-polarized modes [24]. In addition to TM-polarized WGMs with the lowest radial mode number $n = 1$ which circulate closest to the droplet surface, radial LC droplets can also support higher-order radial modes with $n = 2$; these higher-order radial modes typically display lower Q-factors than $n = 1$ modes [11,24].

For bipolar orientation of the LC director [Figs. 4(b) and 4(d)–4(f)], spherical symmetry of the resonator is lost. Thus, modes with the same angular mode number l, but different azimuthal mode numbers m, propagating in planes of different tilt angle with respect to the droplet equatorial plane [42], experience different profiles of refractive index during their propagation around the droplet. Consequently, frequency degeneracy of WGMs observed in Fig. 4(a) is lifted and modes with $l \neq m$ appear at different wavelengths [43,44]. This degeneracy lifting manifests itself as splitting of single spectral peaks into peak families whose precise structure including mode spacing and relative intensities depends on the actual internal profile of the refractive index within the droplet.

Finally, for isotropic-phase droplets [Fig. 4(c)] observed at elevated temperatures, long-range order of LC molecules is completely lost due to Brownian motion and the LC droplets essentially behave like droplets of regular liquids. In particular, birefringence disappears and both TM-polarized and TE-polarized modes with comparable intensities can be now supported. Absence of long-range order also restores complete spherical symmetry of the droplet and, thus, the WGMs become again frequency-degenerate [11].

We note that in our experiments with various LC droplet-based cavities of diameters ranging from ~8 μm to ~25 μm, lasing WGMs were routinely excited using pump pulse energies comparable to those used in our previously reported spectroscopic experiments with droplets of ordinary liquids [17,38]. Thus, the WGM quality factors were not detrimentally affected by residual thermal fluctuations of the local orientation of the LC molecular director.

4. TUNING OF WGM EMISSION SPECTRA OF OPTICALLY TRAPPED LC DROPLETS DUE TO THERMALLY INDUCED PHASE TRANSITIONS IN THE DROPLETS

Using the techniques for controlling the droplet temperature described in Section 2, we characterized the changes of WGM emission spectra of LC droplets accompanying phase transitions of the droplets from the liquid-crystalline phase (temperature below the LC clearing point) into the isotropic phase (temperature above the LC clearing point) and back. To this end, 5CB LC with 1% w/w Nile Red dye was emulsified in 4 mM SDS/water host liquid. As described in Section 3, this combination of materials produces LC droplets in the radial liquid-crystalline phase at the ambient room temperature around ~23°C.

Figure 5 presents typical fluorescence emission spectra recorded from an optically trapped LC droplet of approximately 13.5 μm diameter at different stages of the heating/cooling cycle that was carried out using the microfluidic chip shown in Fig. 2. The actual chip temperatures at which individual spectra were acquired are indicated in the plot headings. Insets in each spectrum show the corresponding images of

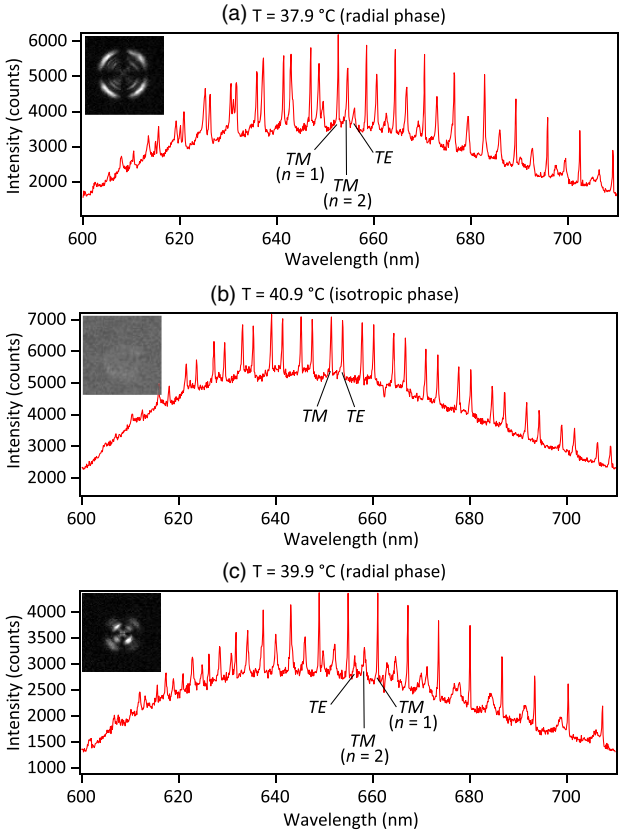

Fig. 5. Tuning of WGM emission spectrum of an optically trapped LC droplet during thermally induced, reversible phase transition. (a) WGM spectrum of a radial LC droplet acquired before melting of the liquid-crystalline phase. (b) WGM spectrum of the same droplet as in (a) acquired after the droplet melting. The droplet is in the isotropic phase. (c) WGM spectrum of the same droplet as in (a) acquired after the droplet cooling. The droplet is in the radial LC phase. Graph insets show corresponding polarization microscopy images of the droplet. For detailed explanation, see discussion in the text.

the studied droplet acquired using polarization microscopy, which reports on the internal organization of LC molecules within the droplet. In the radial LC phase where the molecular director is highly organized, pointing radially away from the center of the droplet, the image of the droplet has a symmetric cross-shaped appearance. At the same time, the droplet WGM emission spectrum features TM-polarized modes of radial orders $n = 1, 2$ and also TE-polarized modes of the lowest radial order $n = 1$ [Fig. 5(a)]. Due to the low contrast between the ordinary refractive index of liquid crystal molecules n_o experienced by TE modes and refractive index of the surrounding host medium n_{host}, the intensities and Q-factors of TE modes are lower than those observed for TM modes (see discussion in Section 3 for details). Upon melting and transition into the isotropic phase, which occurs when the clearing temperature of ~40.1°C is reached, droplet birefringence resulting from the long-range order of LC molecules vanishes and the droplet observed through the crossed polarizer and analyzer becomes practically invisible [Fig. 5(b)]. At the same time, TM-polarized modes with $n = 2$ disappear and the intensities and Q-factors of TE-polarized modes with radial order $n = 1$ become comparable to those of the corresponding TM modes. This behavior stems from the fact that both TE- and TM-mode families now sense the same average refractive index n_{LC} of the isotropic phase LC, where $n_o < n_{\text{LC}} < n_e$. When the temperature is lowered below the clearing point and the droplet transitions back to the liquid-crystalline phase, its internal structure becomes visible again and its spectrum returns to the original WGM pattern with high intensity and high Q-factor TM-polarized modes of various radial orders and low intensity and low Q-factor TE-polarized modes of the lowest radial order [Fig. 5(c)].

The complete temperature-tuning cycle, example spectra from which are shown in Fig. 5, is summarized in the two-dimensional spectral plot of Fig. 6. In this temperature-tuning cycle, emulsion temperature first gradually increased from ~37.5°C to ~41.1°C (time interval 0–110 s), crossing the LC clearing point of ~40.1°C at the time $t \approx 82$ s. After reaching the peak value at the time $t \approx 110$ s, the temperature started decreasing, crossed the point of the transition from isotropic to nematic phase (I → N transition) at the time $t \approx 129$ s, and reached the final value of ~39.9°C at the time $t \approx 165$ s. During the whole experiment, all modes displayed a drift to the blue end of the spectrum, which could be attributed to the gradual droplet dissolution in the host liquid [44]. This drift was estimated from the spectral shift of droplet WGMs in the isotropic phase as -5.2×10^{-3} nm per frame, which translates into the average drift rate of −0.160 nm/s, taking into account inter-frame delay time of 33.3 ms. Besides this dissolution-related effect, a closer look at the two-dimensional spectral plot of Fig. 6 reveals that TM- and TE-polarized modes of radial LC droplets were tuned in opposite directions; with increasing temperature, the wavelength of TM modes decreased whereas the wavelength of TE modes increased, and with decreasing temperature, the tuning directions of the two mode families switched. This trend can be explained by different dependence of the effective ordinary and extraordinary refractive indices n_o, n_e on temperature. When the temperature rises, long-range organization of LC molecules gradually disappears and the ordinary refractive index n_o starts increasing, approaching the value of the isotropic-phase refractive index n_{LC}. Thus, WGMs of the given angular mode number l corresponding to TE-polarized resonances that experience the refractive index n_o are shifted to longer wavelengths. Conversely, gradual loss of LC order causes a decrease of the extraordinary refractive index n_e toward the isotropic-phase value of n_{LC}; hence, TM-polarized resonances, whose spectral positions are dictated by the value of n_e, shift to shorter wavelengths. Naturally, the trends reverse when the temperature decreases. For the part of the tuning cycle in which the temperature increased up to the phase transition point (time $t \approx 82$ s), the average spectral tuning of TM-polarized WGMs with $n = 1$ was estimated as ~6 nm, after correcting the data for the blue-end drift related to the droplet dissolution.

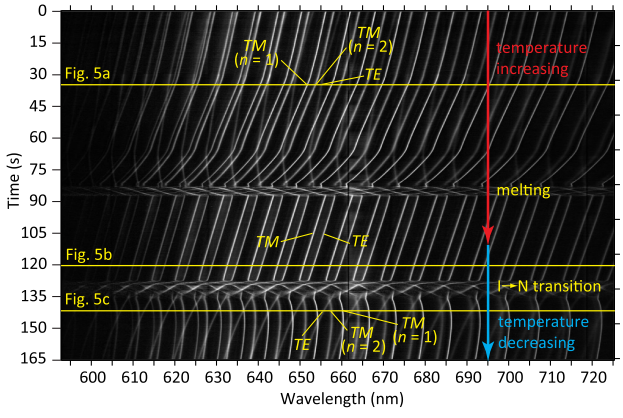

Fig. 6. Complete tuning cycle of WGM emission spectrum of an optically trapped LC droplet induced by controlled temperature changes. Horizontal lines correspond to the LC droplet emission spectra shown in Fig. 5. Labels indicate representative TM- and TE-polarized modes, which display opposite tuning directions during temperature changes.

A visualization illustrating the progress of the full WGM tuning cycle accompanying the reversible thermally induced phase transition of an optically trapped LC droplet from the radial LC phase to the isotropic phase and back is provided in Visualization 1 (see Fig. 7 showing a representative frame from the visualization). This visualization displays simultaneously the actual droplet WGM spectrum, the temperature of the emulsion, and the corresponding polarization image of the droplet acquired during various phases of the melting/cooling process. As shown in the visualization, upon crossing the phase transition points (times $t \approx 82$ s and $t \approx 129$ s), the dynamics of spectral changes becomes very fast, with WGMs rapidly shifting in different directions. These large spectral shifts correlate directly with major variations in the internal structure of the trapped LC droplet revealed by polarization microscopy.

As discussed in Section 2, the temperature of LC droplets can be also controlled locally by changing the power of the trapping beam used to confine the droplets during the experiment. Figure 8 summarizes a typical spectral tuning experiment in which the phase transition from the radial LC phase to the isotropic phase and back was induced in an optically trapped droplet by a gradual modulation of the trapping power. A radial LC droplet (emulsion system 5CB +1% w/w Nile Red +4 mM SDS—see Section 3) with the diameter of ~22 μm was initially

trapped at 30 mW (measured before the microscope) and the trapping power was then slowly ramped up to 2500 mW and back, resulting in one full tuning cycle with each power step lasting 400 ms. During the power modulation, droplet emission spectra and polarization microscopy images were simultaneously acquired to monitor the progress of the phase transition. Analogically to the temperature tuning cycle presented in Fig. 6, the structure of the droplet WGM spectra changes dramatically when the droplet melts. During the phase transition, WGMs of different polarization (TE or TM) excited in the radial LC droplet shift to the opposite ends of the spectrum. Because of the low contrast of the ordinary refractive index n_o in comparison to the extraordinary refractive index n_e, Q-factors of TE modes are lower than those observed for TM modes (see discussion in Section 3 for details). In the isotropic phase, only the lowest radial order modes with $n = 1$ are visible and the intensities and Q-factors of both TE and TM modes become comparable. When the droplet is cooled back to the original temperature, its spectrum displays again the characteristic features of the radial LC phase. The cooling part of the tuning cycle is essentially a mirror image of the heating part. Overall, the observed behavior is identical to that described above for experiments carried out with heated microfluidic chips. However, the present experimental configuration enables much more precise and localized control of the droplet temperature. Since the temperature of the host liquid does not change appreciably when the heating is confined to the vicinity of the trapping beam focus, dissolution of LC droplets in the host liquid is much lower. Consequently, blue-end drift of all WGMs during the course of experiment is much less pronounced than that observed in Fig. 6. In particular, the drift rate in the isotropic phase of the power tuning cycle, with the dwell time of power steps equal to 400 ms, was estimated as –0.025 nm/s, i.e., 6.4-times smaller than the drift rate observed in Fig. 6. The tuning range of TM-polarized WGMs with $n = 1$, corrected for drift, was then approximately 6.1 nm during the power-increasing part of the cycle.

Droplet changes during the phase transition are visualized in more detail in Fig. 9, which shows the spectra recorded

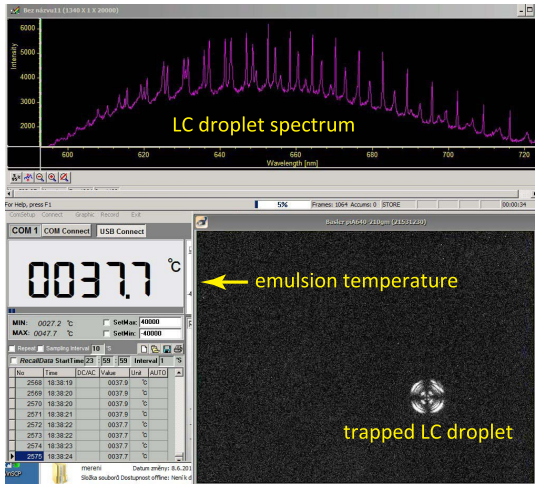

Fig. 7. Monitoring of tuning of WGM emission spectrum of an optically trapped LC droplet induced by controlled temperature changes (see Visualization 1). Droplet spectrum is displayed in the top panel, together with the corresponding temperature of the emulsion (bottom left panel) and polarization image of the studied droplet (bottom right panel). In the shown sample frame from the visualization, the droplet is in the radial LC phase.

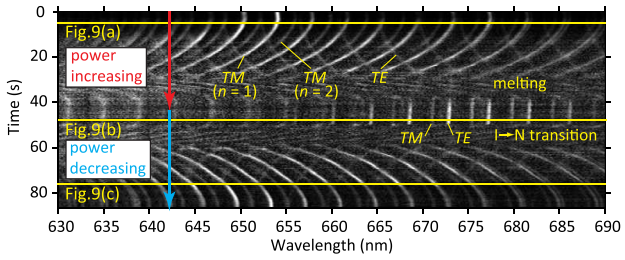

Fig. 8. Complete tuning cycle of WGM emission spectrum of an optically trapped LC droplet induced by controlled changes of trapping power. Horizontal lines correspond to the LC droplet emission spectra shown in Fig. 9. Labels indicate representative TM- and TE-polarized modes, which display opposite tuning directions during temperature changes.

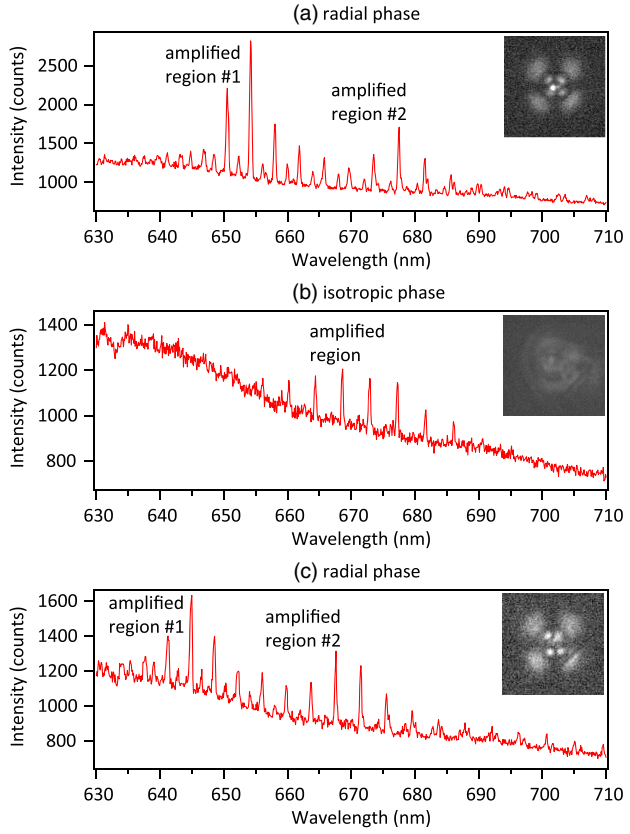

Fig. 9. Tuning of WGM emission spectrum of an optically trapped LC droplet during reversible phase transition induced by gradual changes of the trapping power. (a) WGM spectrum of a radial LC droplet acquired before melting of the liquid-crystalline phase. (b) WGM spectrum of the same droplet as in (a) acquired after the droplet melting. The droplet is in the isotropic phase. (c) WGM spectrum of the same droplet as in (a) acquired after the droplet cooling. The droplet is in the radial LC phase. Graph insets show corresponding polarization microscopy images of the droplet. For detailed explanation, see discussion in the text.

at various stages of the heating/cooling process together with the corresponding polarization-microscopy images of the droplet. Here, a cross-shaped image of the droplet indicates the radial LC phase whereas a smeared, irregular image indicates the isotropic phase. Comparison of Figs. 9(a) and 9(c) with Fig. 9(b) reveals selective amplification of WGMs in different parts of the emission spectrum for different LC phases: while for radial LC droplets, two distinct spectral regions of WGM amplification are observed, only one spectral region with amplified WGMs is visible when the droplet melts into the isotropic phase. Thus, with localized heating, structural changes in LC droplets can be monitored in greater detail and spectroscopic measurements—in combination with polarization microscopy of the droplets—can potentially serve as a sensitive indicator of phase transition processes taking place in LC droplets.

5. TUNING OF WGM EMISSION SPECTRA OF OPTICALLY TRAPPED ISOTROPIC LC DROPLETS

Even for isotropic emulsion droplets of regular liquids, temperature variations are generally accompanied by changes of the refractive index and size of the droplet, which subsequently lead to bidirectional shifts of the droplet resonant wavelength [17]. In order to study the thermally induced spectral tuning of WGMs of isotropic LC droplets, we carried out a series of experiments in which fluorescence emission spectra were recorded from individual droplets confined in optical tweezers with gradually modulated trapping power. Figure 10 shows representative spectral tuning curves obtained from a single optically trapped isotropic LC droplet (emulsion system 5CB +0.3% w/w Nile Red +1200 mg/L Triton X-100) with a diameter of ∼19 μm by modulating periodically the trapping power between 240 mW and 720 mW in two full modulation cycles. In the four measurement series shown in Fig. 10, the droplet was optically trapped inside an ITO-coated capillary (see Fig. 3) and the dwell time τ for each power step in the cycle was changed from 3000 ms [Fig. 10(a)] up to 10000 ms [Fig. 10(d)]. Dashed and solid vertical lines labeled λ_{min}, λ_{max} connect the positions of minimal and maximal wavelengths, respectively, of a representative WGM obtained in successive power modulation cycles. Comparison of spectral tuning curves obtained with different dwell times reveals clearly increasing amplitude of tuning with increasing dwell time. In particular, WGM tuning amplitudes were 3.1 nm for $\tau = 3000$ ms, 4.0 nm for $\tau = 5000$ ms, 4.8 nm for $\tau = 7000$ ms, and 6.3 nm for $\tau = 10000$ ms. We hypothesize that the large observed spectral tuning of optically trapped isotropic LC droplets, which cannot be fully explained just by the direct thermally induced changes of the size and refractive index of the droplet, is predominantly caused by temperature-dependent, dynamic partitioning of Triton X-100 between the host and droplet liquids [45]. Diffusive transport of Triton X-100 across the interface between the host and droplet liquids results in a spatially and temporally varying concentration profile of the surfactant within the droplet accompanied by modulation of the droplet's refractive index. This change in the optical properties of the droplet then leads to the shifting of spectral positions of its WGMs. The temperature of the droplet during the power-tuning cycle reaches equilibrium within a few tens of milliseconds [17]. However, since the solubility of Triton X-100 in the LC fluid is limited, the kinetics of net molecular transport of surfactant molecules into and out of the LC droplet is comparably slower [46]. Consequently, with longer dwell times allowed during the power-tuning cycle, larger surfactant-induced changes of the droplet's optical properties can be achieved, which translate into a larger observed spectral tuning range. We note that even with the longest dwell time corresponding to the largest tuning range, observed tuning is still almost fully reversible, i.e., it is not caused by LC dissolution in the host liquid.

While ITO-coated glass capillary enables (almost) fully reversible spectral tuning of droplet WGMs over more than 6 nm with relatively low trapping power, confinement of LC droplets in the optical trap is more challenging in this

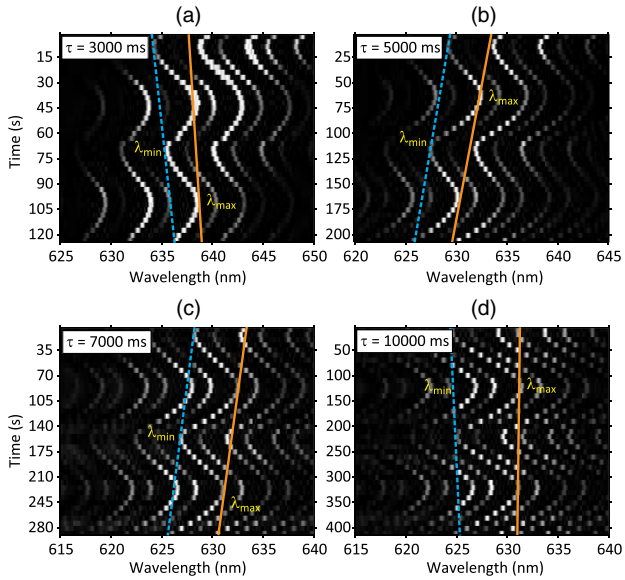

Fig. 10. Spectral tuning of emission from an isotropic LC droplet optically trapped in ITO-coated capillary by changing the power of the trapping laser beam. For all spectra, two full cycles of power modulation were carried out, in which the trapping power before the microscope changed periodically from 240 mW to 720 mW in 10 steps with different dwell times τ of each power step. (a) $\tau = 3000$ ms, (b) $\tau = 5000$ ms, (c) $\tau = 7000$ ms, (d) $\tau = 10000$ ms.

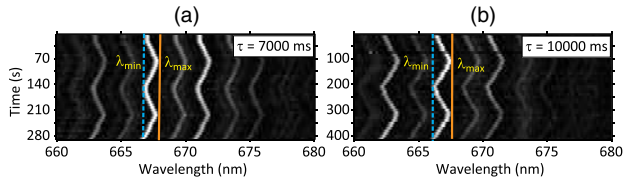

Fig. 11. Spectral tuning of emission from an isotropic LC droplet optically trapped in a microfluidic chip by changing the power of the trapping laser beam. For both spectra, two full cycles of power modulation were carried out, in which the trapping power before the microscope changed periodically from 1200 mW to 2400 mW in 10 steps with different dwell times τ for each power step. (a) $\tau = 7000$ ms, (b) $\tau = 10000$ ms.

configuration, as the differential heating of the sample chamber leads to strong thermally induced liquid convection in the capillary, which destabilizes the trapping. In order to eliminate the disturbing effect of host liquid convection, we repeated the power tuning experiments using the same emulsion system suspended in a microfluidic chip. Figure 11 shows a typical result of such tuning experiments for an LC droplet with a diameter of ~20 μm. Due to the absence of absorptive ITO layers, significantly higher trapping power must be used (average tuning power for the chip was 1800 mW while the average tuning power for the ITO-coated capillary was 480 mW) and the observed tuning range is smaller (0.9 nm for $\tau = 7000$ ms and 1.3 nm for $\tau = 10000$ ms). On the other hand, droplet trapping is much more stable and—in addition—residual dissolution of the trapped LC droplet in the host liquid is strongly suppressed. In practice, it should be possible to find an optimal thickness of ITO coating deposited on the capillary walls, which would allow for a spectral tuning range of several nanometers with moderate trapping power, without pronounced destabilizing effects of the host liquid convection.

6. CONCLUSION

We have studied tunable optofluidic microcavities formed by six different types of dye-doped emulsion droplets of nematic liquid crystals suspended in an aqueous host liquid and confined in optical tweezers. We have shown that WGM emission spectra of such droplet resonators can be monitored over extended time periods, having recorded several thousands of spectra from a single droplet. By changing periodically the temperature of the droplet, we have demonstrated that the WGM spectra of the droplet resonators can be largely tuned in both directions. Specifically, for radial LC droplets with SDS surfactant undergoing reversible phase transitions between the liquid-crystalline and isotropic phase, the maximal observed tuning range corrected for drift was ~6.1 nm, whereas for isotropic LC droplets with Triton X-100 surfactant, the maximal observed tuning range was ~6.3 nm. Residual irreversibility observed in the spectral tuning patterns can be potentially reduced or even completely eliminated by optimizing the composition of the host liquid supporting the droplets (mainly the type and/or concentration of the used surfactant). The presented results indicate feasibility of this approach for creating miniature largely tunable sources of coherent light that can be manipulated and stabilized by optical forces. If the cavity temperature is controlled locally (e.g., by adjusting the power of the trapping laser beam), one can envision implementing a (relatively fast) feedback loop that will keep the emission wavelength of the cavity locked to the target value. In addition, spectroscopic measurements with LC droplets subject to external stimuli—in particular, controlled changes of the ambient temperature that eventually induce phase transitions in the droplets—can elucidate the processes taking place in the droplets during external perturbations. Such studies carried out with LC arrangements different from typically studied LC geometries (bulk fluids or thin 2D films) can contribute to the fundamental research in the field of liquid crystal physics.

Funding. Türkiye Bilimsel ve Teknolojik Araştirma Kurumu (TÜBİTAK) (114F253); Akademie věd České republiky (TÜBİTAK 14-006); European Cooperation in Science and Technology (COST) (MP1205); Ministerstvo školství, mládeže a tělovýchovy (MŠMT) (LD14069, LO1212); European Commission (EC) (CZ.1.05/2.1.00/01.0017).

Acknowledgment. The authors thank J. Oulehla (Institute of Scientific Instruments) for technical assistance with preparing capillary-based sample chambers used in selected experiments.

REFERENCES

1. C. Monat, P. Domachuk, and B. J. Eggleton, "Integrated optofluidics: a new river of light," Nat. Photonics **1**, 106–114 (2007).
2. X. Fan and I. M. White, "Optofluidic microsystems for chemical and biological analysis," Nat. Photonics **5**, 591–597 (2011).
3. K. J. Vahala, "Optical microcavities," Nature **424**, 839–846 (2003).
4. H. Azzouz, L. Alkhafadiji, S. Balslev, J. Johansson, N. A. Mortensen, S. Nilsson, and A. Kristensen, "Levitated droplet dye laser," Opt. Express **14**, 4374–4379 (2006).
5. A. Kiraz, A. Sennaroglu, S. Doganay, M. A. Dundar, A. Kurt, H. Kalaycioglu, and A. L. Demirel, "Lasing from single, stationary, dye-doped glycerol/water microdroplets located on a superhydrophobic surface," Opt. Commun. **276**, 145–148 (2007).
6. S. Nizamoglu, M. C. Gather, and S. H. Yun, "All-biomaterial laser using vitamin and biopolymers," Adv. Mater. **25**, 5943–5947 (2013).
7. A. Jonáš, M. Aas, Y. Karadağ, S. Manioğlu, S. Anand, D. McGloin, H. Bayraktar, and A. Kiraz, "In vitro and in vivo biolasing of fluorescent proteins suspended in liquid microdroplet cavities," Lab Chip **14**, 3093–3100 (2014).
8. H. Zhang, A. Balram, D. D. Meng, and Y. Sun, "Optofluidic lasers with monolayer gain at the liquid-liquid interface," ACS Photon. **4**, 621–625 (2017).
9. V. V. Datsyuk, "Optics of microdroplets," J. Mol. Liq. **84**, 1308–1316 (2001).
10. A. Giorgini, S. Avino, P. Malara, P. D. Natale, and G. Gagliardi, "Fundamental limits in high-Q droplet microresonators," Sci. Rep. **7**, 41997 (2017).
11. G. C. Righini, Y. Dumeige, P. Feron, M. Ferrari, G. N. Conti, D. Ristic, and S. Soria, "Whispering gallery mode microresonators: fundamentals and applications," Riv. Nuovo Cimento **34**, 435–488 (2011).
12. S.-X. Qian, J. B. Snow, H. M. Tzeng, and R. K. Chang, "Lasing droplets: highlighting the liquid-air interface by laser emission," Science **231**, 486–488 (1986).
13. A. Kiraz, A. Kurt, M. A. Dündar, and A. L. Demirel, "Simple largely tunable optical microcavity," Appl. Phys. Lett. **89**, 081118 (2006).
14. A. Kiraz, Y. Karadağ, and A. F. Coskun, "Spectral tuning of liquid microdroplets standing on a superhydrophobic surface using electrowetting," Appl. Phys. Lett. **92**, 191104 (2008).
15. A. Kiraz, Y. Karadag, S. C. Yorulmaz, and M. Muradoglu, "Reversible photothermal tuning of a salty water microdroplet," Phys. Chem. Chem. Phys. **11**, 2597–2600 (2009).
16. S. C. Yorulmaz, M. Mestre, M. Muradoglu, B. E. Alaca, and A. Kiraz, "Controlled observation of nondegenerate cavity modes in a microdroplet on a superhydrophobic surface," Opt. Commun. **282**, 3024–3027 (2009).
17. M. Aas, A. Jonáš, A. Kiraz, O. Brzobohatý, J. Ježek, Z. Pilát, and P. Zemánek, "Spectral tuning of lasing emission from optofluidic droplet microlasers using optical stretching," Opt. Express **21**, 21380–21394 (2013).
18. V. Ta, R. Chen, and H. Sun, "Tuning whispering gallery mode lasing from self-assembled polymer droplets," Sci. Rep. **3**, 1362 (2013).
19. S. Avino, A. Krause, R. Zullo, A. Giorgini, P. Malara, P. D. Natale, H. P. Loock, and G. Gagliardi, "Direct sensing in liquids using whispering-gallery-mode droplet resonators," Adv. Opt. Mater. **2**, 1155–1159 (2014).

20. L. Labrador-Páez, K. Soler-Carracedo, M. Hernández-Rodríguez, I. R. Martín, T. Carmon, and L. L. Martin, "Liquid whispering-gallery-mode resonator as a humidity sensor," Opt. Express **25**, 1165–1172 (2017).
21. T. Lopez-Leon and A. Fernandez-Nieves, "Drops and shells of liquid crystal," Colloid Polym. Sci. **289**, 345–359 (2011).
22. I. Muševič, "Nematic colloids, topology, and photonics," Philos. Trans. R. Soc. A **371**, 20120266 (2013).
23. M. Urbanski, C. Reyes, J. Noh, A. Sharma, Y. Geng, V. Jampani, and J. Lagerwall, "Liquid crystals in micron-scale droplets, shells and fibers," J. Phys. **29**, 133003 (2017).
24. M. Humar, M. Ravnik, S. Pajk, and I. Muševič, "Electrically tunable liquid crystal optical microresonators," Nat. Photonics **3**, 595–600 (2009).
25. M. Humar and I. Muševič, "Surfactant sensing based on whispering-gallery-mode lasing in liquid-crystal microdroplets," Opt. Express **19**, 19836–19844 (2011).
26. J. Li, S. Gauza, and S. Wu, "Temperature effect on liquid crystal refractive indices," J. Appl. Phys. **96**, 19–24 (2004).
27. M. Humar, "Liquid-crystal–droplet optical microcavities," Liq. Cryst. **43**, 1937–1950 (2016).
28. Y. Wang, H. Li, L. Zhao, Y. Liu, S. Liu, and J. Yang, "Tapered optical fiber waveguide coupling to whispering gallery modes of liquid crystal microdroplet for thermal sensing application," Opt. Express **25**, 918–926 (2017).
29. T. A. Kumar, M. A. Mohiddon, N. Dutta, N. K. Viswanathan, and S. Dhara, "Detection of phase transitions from the study of whispering gallery mode resonance in liquid crystal droplets," Appl. Phys. Lett. **106**, 051101 (2015).
30. G. P. Crawford and S. Žumer, eds., *Liquid Crystals in Complex Geometries: Formed by Polymer and Porous Networks* (CRC Press, 1996).
31. G. Cipparrone, A. Mazzulla, A. Pane, R. J. Hernandez, and R. Bartolino, "Chiral self-assembled solid microspheres: a novel multifunctional microphotonic device," Adv. Mater. **23**, 5773–5778 (2011).
32. H. Coles and S. Morris, "Liquid-crystal lasers," Nat. Photonics **4**, 676–685 (2010).
33. M. Humar and I. Muševič, "3D microlasers from self-assembled cholesteric liquid-crystal microdroplets," Opt. Express **18**, 26995–27003 (2010).
34. H.-G. Lee, S. Munir, and S.-Y. Park, "Cholesteric liquid crystal droplets for biosensors," ACS Appl. Mater. Interfaces **8**, 26407–26417 (2016).
35. A. Ashkin, J. Dziedzic, J. Bjorkholm, and S. Chu, "Observation of a single-beam gradient force optical trap for dielectric particles," Opt. Lett. **11**, 288–290 (1986).
36. A. Jonáš and P. Zemánek, "Light at work: the use of optical forces for particle manipulation, sorting, and analysis," Electrophoresis **29**, 4813–4851 (2008).
37. S. Kaminski, L. L. Martin, and T. Carmon, "Tweezers controlled resonator," Opt. Express **23**, 28914–28919 (2015).
38. M. Aas, A. Jonáš, and A. Kiraz, "Lasing in optically manipulated, dye-doped emulsion microdroplets," Opt. Commun. **290**, 183–187 (2013).
39. S. K. Hait and S. P. Moulik, "Determination of critical micelle concentration (CMC) of nonionic surfactants by donor-acceptor interaction with iodine and correlation of CMC with hydrophile-lipophile balance and other parameters of the surfactants," J. Surfactants Deterg. **4**, 303–309 (2001).
40. G. A. Oweimreen and D. E. Martire, "The effect of quasispherical and chainlike solutes on the nematic to isotropic phase transition in liquid crystals," J. Chem. Phys. **72**, 2500–2510 (1980).
41. S. Singh, *Liquid Crystals Fundamentals* (World Scientific, 2002).
42. B. Little, J.-P. Laine, and H. Haus, "Analytic theory of coupling from tapered fibers and half-blocks into microsphere resonators," J. Lightwave Technol. **17**, 704–715 (1999).
43. M. Hossein-Zadeh and K. J. Vahala, "Fiber-taper coupling to whispering-gallery modes of fluidic resonators embedded in a liquid medium," Opt. Express **14**, 10800–10810 (2006).
44. A. Jonáš, Y. Karadag, M. Mestre, and A. Kiraz, "Probing of ultrahigh optical *Q*-factors of individual liquid microdroplets on superhydrophobic surfaces using tapered optical fiber waveguides," J. Opt. Soc. Am. B **29**, 3240–3247 (2012).
45. M. Schick, ed., *Nonionic Surfactants: Physical Chemistry* (Marcel-Dekker, 1987).
46. P. M. Gassin, G. Martin-Gassin, D. Meyer, J.-F. Dufrêche, and O. Diat, "Kinetics of Triton-X100 transfer across the water/dodecane interface: analysis of the interfacial tension variation," J. Phys. Chem. C **116**, 13152–13160 (2012).